Mean field and Monte Carlo analysis of the p-state chiral clock model

1989 J. Phys. A: Math. Gen. 22 4463

(http://iopscience.iop.org/0305-4470/22/20/022)

J. Phys. A: Math. Gen. **22** (1989) 4463–4476. Printed in the UK

Mean field and Monte Carlo analysis of the p-state chiral clock model

W Scott McCullough and H L Scott

Department of Physics, Oklahoma State University, Stillwater, OK 74078-0444, USA

Received 14 April 1989

Abstract. We present the results of calculations of the phase properties of the p-state chiral clock model for $p = 4$ and 8 using the mean-field approximation and the Monte Carlo method. Phase diagrams are calculated using both methods and the results are compared. Within the mean-field approximation it is possible to determine the structures of the stable phases to very high precision by a systematic process similar to that used for the ANNNI model by others. The mean-field calculations show that the number of stable phases increases as p increases, and that away from the multiphase point new phases are formed from combinations of the stable low-temperature phases. Monte Carlo phase diagrams are determined from the properties of the averages of the Potts spins along the chiral axis. These diagrams are in qualitative agreement with the mean-field diagrams. The Monte Carlo calculations reveal a modulated phase region which increases in complexity as p increases, but the simulations are not able to yield simple precise modulated structures.

1. Introduction

The three-state chiral clock model [1, 2] is the simplest model involving only nearest-neighbour (NN) interactions which exhibits modulated phases. As a consequence this model has been studied extensively by exact low-temperature series expansions [3], mean-field theory [4, 5], the Bethe approximation [6], the Monte Carlo method [7] and renormalisation group theory [2]. The basic features of the phase diagram of this model are thus well understood [8]. In contrast, less is known about the phase diagram of the more general p-state chiral clock (CC_p) model [9] for $p > 3$. This is due in part to a lack of clear theoretical or experimental motivation to carry out the more difficult analysis of the model with larger p. Recently however, Scott and Pearce [10] introduced a new model for the $P_{\beta'}$ phase in lipid bilayers which is closely related to the CC_p model with $p \simeq 8$. In the lipid bilayer model the modulated phase is one in which the surface of the otherwise planar two-dimensional bilayer becomes 'corrugated' with periodic (but asymmetric) ripple-like structure [11]. In the model of Scott and Pearce the modulated phase region is associated with the ripples in the $P_{\beta'}$ phase.

This has led us to undertake a study of the CC_p model for $p = 4$ and $p = 8$ using mean-field theory and the Monte Carlo method. In the following section we introduce the model, describe the mean-field calculations and give the principal features of the phase diagram which result from this approximation. In § 3 the Monte Carlo method and results will be described. In § 4 we compare the results from the two different analyses.

0305-4470/89/204463+14$02.50

2. Mean-field theory

2.1. Basic aspects of the model and notation

The CC_p model is defined on a hypercubic lattice of dimension d by the Hamiltonian

$$\mathscr{H} = -\sum_z \sum_{\langle i,j \rangle} \left[J_0 \boldsymbol{\sigma}_{i,z} \cdot \boldsymbol{\sigma}_{j,z} + J \boldsymbol{\sigma}_{i,z} \cdot R(-\Delta) \boldsymbol{\sigma}_{i,z+1} \right] \tag{1}$$

where J_0 is the ferromagnetic interaction energy for nearest-neighbour (NN) pairs in the $(d-1)$-dimensional layers and J is the interaction energy between nearest-neighbour pairs along the chiral axis, z. The notation $\langle i,j \rangle$ indicates that the sum is to be carried out over NN pairs only. The $\{\boldsymbol{\sigma}_{i,z}\}$ are two-dimensional vectors defined by

$$\boldsymbol{\sigma}_{i,z} \equiv \left(\cos(2\pi n_{i,z}/p),\ \sin(2\pi n_{i,z}/p) \right)$$

where the Potts variable $n_{i,z}$ can take on the values $n_{i,z} = 0, 1, \ldots, p-1$. The operator R is the two-dimensional rotation matrix

$$R(\Delta) = \begin{bmatrix} \cos 2\pi\Delta/p & -\sin 2\pi\Delta/p \\ \sin 2\pi\Delta/p & \cos 2\pi\Delta/p \end{bmatrix}. \tag{2}$$

The effect of the chiral field Δ can be seen by considering the ground states of the model for $0 \leq \Delta \leq 1$. Note that it is sufficient to consider the relative ordering of successive spins along the chiral axis z since from equation (1) it is clear that the lowest-energy state of the model is one in which all the Potts variables in a given layer take on the same value, regardless of the choice of Δ. For $0 \leq \Delta < 1/2$ the ground state is one in which the Potts variables along the z axis take on identical values. This phase is commonly denoted by $\langle \infty \rangle$. When $1/2 < \Delta \leq 1$ the ground state is one of *chiral order* along the z axis. That is, the successive Potts variables along this axis increase by $+1$ in sequence, $n_{i,z} = 0\ 1\ 2\ \ldots\ (p-1)\ 0\ 1 \ldots$. Employing the notation of Yeomans and Fisher [3], this phase is denoted by $\langle 1 \rangle$. At the point $\Delta = 1/2$, the energy of interaction is the same for adjacent Potts spins which have $n_{z+1} = n_z$ or $n_{z+1} = n_z + 1$ so that the ground state at this point is infinitely degenerate. The point $T = 0$, $\Delta = 1/2$ is thus a *multiphase point*.

Above $T = 0$ the nature of the phases in the three-dimensional model which can coexist near $\Delta = 1/2$ has been determined for $p = 3$ by Yeomans and Fisher [3] by analysis of exact low-temperature series expansions. The principal result is that for $\Delta \gtrsim 1/2$, the $\langle 1 \rangle$ phase is eventually replaced, as T increases, by a phase in which the sites along the z axis follow the ordering pattern ...011200122..., i.e. a chiral bond followed by a ferromagnetic bond, repeating along the z axis. The abbreviation for this phase is $\langle 12 \rangle$. If Δ is not too large the $\langle 12 \rangle$ phase is followed (as temperature increases) by a $\langle 122 \rangle$ (or $\langle 12^2 \rangle$) phase, and then $\langle 12^3 \rangle$, etc. The temperature regions in which phases of the form $\langle 12^j \rangle$ are stable become smaller as Δ approaches 1/2 from above. From the pattern established for $\Delta > 1/2$ one can also construct directly the phase sequence for $\Delta < 1/2$ from the fact that the partition function of the CC_p model is invariant under the transformation [9]

$$\Delta \to 1 - \Delta \qquad n_z \to -n_z + z \pmod{p}. \tag{3}$$

For $p > 3$ analysis of the exact low-temperature series for the three-dimensional model indicates that stable phases of the form $\langle 1^j 2\rangle$ intervene between the $\langle 1\rangle$ and the $\langle 12\rangle$ phases as long as $j \leq p-2$. Further, as T increases, the $\langle 12^j\rangle$ sequence of phases gives way to additional phases. For example, for $p = 4$, the sequence of stable phases near $\Delta = 1/2$ as T increases is found to be [9]

$$\langle 1\rangle \to \langle 1^2 2\rangle \to \langle 12\rangle \to \langle 1212^2\rangle \to \langle 12^2\rangle$$
$$\to \langle 12^2 12^3\rangle \to \langle 12^3\rangle \to \langle 12^3 12^4\rangle \to \ldots \to \langle 2\rangle.$$

Mean field [4, 5] and Bethe approximations [6] have also been applied to the three-dimensional CC_3 model. At low temperatures it is found [5] that the mean-field approximation yields more commensurate phases than are found in the analysis of the exact low-temperature series. The Bethe approximation, however, precisely reproduces [6] the sequence of low-temperature phases found from the exact low-temperature series [3].

In contrast to the discrete nature of the low-temperature commensurate phases, the stable phases in the vicinity of the order–disorder line T_c are incommensurate and are characterised by a continuously varying wavevector. In the interesting—and physically relevant—intermediate region between $T = 0$ and $T \simeq T_c$ the nature of the stable phases is not as well known. To date, the mean-field [4, 5] and Bethe approximations [6] have been applied only to the $p = 3$ model in three dimensions. In this region the two methods give approximately the same phase sequences and branching points of new commensurate phases [6], which suggests that the mean-field approximation is better for higher temperatures. The temperature scales differ for the two methods, with mean-field temperatures higher, as is usually the case.

2.2. *Mean-field equations*

To obtain the mean-field free energy G_{mf} of the two-dimensional CC_p model we use the variational principle afforded by the Gibbs–Bogoliubov inequality [12],

$$G \leq G_{mf} = \min\left[G_0 + \langle \mathscr{H} - \mathscr{H}_0\rangle_0\right] \tag{4}$$

where G is the exact free energy, $\mathscr{H}_0$ is any trial Hamiltonian, and the average denoted by $\langle\ \rangle_0$ is carried out in the $\mathscr{H}_0$ ensemble. The procedure is completely analogous to that carried out for the ANNNI model by Yokoi *et al* [13] and for the CC_3 model by Öttinger [4]. In this way we find for the CC_p model on an $N \times N$ two-dimensional lattice with chiral interactions along the z axis the result

$$\frac{G_{mf}}{N^2} = \frac{1}{N}\sum_{z=1}^{N}\left[J_0 \boldsymbol{m}_z \cdot \boldsymbol{m}_z + J\boldsymbol{m}_z \cdot R(\Delta)\boldsymbol{m}_{z-1} - T\ln\left(\sum_{n=0}^{p-1}\exp(\beta\boldsymbol{\eta}_z \cdot \boldsymbol{\sigma}(n))\right)\right] \tag{5}$$

where $\boldsymbol{m}_z$ is the average magnetisation in a 'layer', defined by

$$\boldsymbol{m}_z = N\frac{\sum_{n=0}^{p-1}\boldsymbol{\sigma}(n)\exp(\beta\boldsymbol{\eta}_z \cdot \boldsymbol{\sigma}(n))}{\sum_{n=0}^{p-1}\exp(\beta\boldsymbol{\eta}_z \cdot \boldsymbol{\sigma}(n))} \tag{6}$$

and

$$\boldsymbol{\eta}_z = 2J_0\boldsymbol{m}_z + J\left(R(\Delta)\boldsymbol{m}_{z-1} + R(-\Delta)\boldsymbol{m}_{z+1}\right) \tag{7}$$

is the mean field in 'layer' z. For a given choice of T and Δ the stable phase is the one that minimises G_{mf}, and this phase is given by the solution of the set of (non-linear) equations (6), with $\boldsymbol{\eta}_z$ given by equation (7).

2.3. Numerical solution of the mean-field equations

Let us now turn to the problem of determining the stable commensurate phases for intermediate temperatures between $T = 0$ and the order–disorder line $T = T_c$ by solving equations (6) numerically on finite lattices. Suppose we obtain, for a given choice of T and Δ, a configuration that minimises G_{mf} on a lattice with L layers. This configuration may not be the stable phase on the infinite lattice; a similar solution for a lattice with, say, $L + 2$ layers may give a smaller value for G_{mf}. Thus to find the commensurate phase which minimises G_{mf} it is necessary to compare the free energy for solutions of equations (6) on lattices of all possible sizes.

To circumvent this impossibility, we employ a 'systematic finite-lattice mean-field' approach proposed originally by Selke and Duxbury for the ANNNI model [14]. In this approach the phase diagram for intermediate temperatures is deduced in a self-consistent way by supposing that additional, more complicated commensurate phases are formed from combinations of the basic commensurate phases that spring from the multiphase point. The mean-field equations (6) are then solved iteratively, for each hypothesised phase, on the smallest lattice (with periodic boundary conditions) which is compatible with the phase in question. The free energies per site of each phase are then computed and compared to find the stable phase. In this way it is possible to determine the minimum free energy by considering only a small subset of finite lattice sizes.

Since the precise sequence of phases which springs from the multiphase point of the two-dimensional CC_p model in the mean-field approximation is not known, we have modified the systematic mean-field finite-lattice approach in a way we now describe. We begin by assuming for $T > 0$ the stability of only the $\langle 1 \rangle$, $\langle 12 \rangle$ and $\langle 2 \rangle$ phases at the multiphase point. Then for each Δ we find the temperature at which the $\langle 1 \rangle$ phase becomes unstable with respect to the $\langle 12 \rangle$ phase, and the temperature at which $\langle 12 \rangle$ phase becomes unstable with respect to the $\langle 2 \rangle$ phase (this latter boundary exists for sufficiently small Δ). With these pseudo phase boundaries established we then check to see if the $\langle 1 \rangle$:$\langle 12 \rangle$ and $\langle 12 \rangle$:$\langle 2 \rangle$ phase boundaries are unstable with respect to the presence of the $\langle 1^2 2 \rangle$ and $\langle 12^2 \rangle$ phases, respectively. The phases $\langle 1^2 2 \rangle$ and $\langle 12^2 \rangle$ may be thought of as combinations of the $\langle 1 \rangle$ and $\langle 12 \rangle$ phases, and the $\langle 12 \rangle$ and $\langle 2 \rangle$ phases, respectively. The process is repeated until the previously established phase boundaries are found to be stable to the hypothesised presence of the 'new' phases. We illustrate the first few levels of this systematic search in table 1.

Table 1. Successive search levels for pseudo phase boundaries in the systematic finite-lattice mean-field approach to the CC_p model. Each colon denotes the boundary between the two phases.

$\langle 1 \rangle : \langle 2 \rangle$
$\langle 1 \rangle : \langle 12 \rangle : \langle 2 \rangle$
$\langle 1 \rangle : \langle 1^2 2 \rangle : \langle 12 \rangle : \langle 12^2 \rangle : \langle 2 \rangle$
$\langle 1 \rangle : \langle 1^3 2 \rangle : \langle 1^2 2 \rangle : \langle 1^2 212 \rangle : \langle 12 \rangle : \langle 1212^2 \rangle : \langle 12^2 \rangle : \langle 12^3 \rangle : \langle 2 \rangle$
$\langle 1 \rangle : \langle 1^4 2 \rangle : \langle 1^3 2 \rangle : \langle 1^3 21^2 2 \rangle : \langle 1^2 2 \rangle : \langle (1^2 2)^2 12 \rangle : \langle 1^2 212 \rangle : \langle 1^2 2(12)^2 \rangle : \langle 12 \rangle :$ $\langle (12)^2 12^2 \rangle : \langle 1212^2 \rangle : \langle 12(12^2)^2 \rangle : \langle 12^2 \rangle : \langle 12^2 12^3 \rangle : \langle 12^3 \rangle : \langle 12^4 \rangle : \langle 2 \rangle$

Several details concerning the numerical method are worth noting. First, we used a multivariable generalisation of Newton's iteration method [15] to solve the system of non-linear equations (6). Each hypothesised phase was chosen as an initial configuration on a lattice of appropriate size and equations (6) were then iterated to convergence. The use of Newton's method ensured rapid convergence of the iterations even for temperatures near the order–disorder temperature T_c. Because of this we were able to consider commensurate phases which required lattice sizes of up to $\simeq 130$ sites. Furthermore the method proved to be capable of very high accuracy—up to 31 or 32 decimal digits—when carried out on computers which support very high precision (128 bits) arithmetic. This proved to be necessary near the multiphase point where free-energy differences between adjacent stable phases approach zero as Δ approaches 1/2. The analysis of the eight-state model required this high precision even away from the multiphase point since, for comparable values of Δ, the temperature region in which a phase is stable is much smaller than for $p = 3$ or $p = 4$.

2.4. *Phase diagrams*

The large-scale features of the T–Δ phase diagram for the CC_4 model (with $J_0 = J$) which emerge from the systematic finite-lattice mean-field computations are shown in figure 1 (broken curves) together with the results of the Monte Carlo simulations (full lines) to be described later. The upper broken curve is the mean-field order–disorder line $T_c = 2J/k_B$, which is obtained easily from the determination of the mean field T_c for the *three-dimensional* CC_p model [4]. The lower broken curve was obtained by solving the mean-field equations (6) directly for the case $\Delta > 1/2$. The results for $\Delta < 1/2$ were then obtained by reflecting the results for $\Delta > 1/2$ using the symmetry properties of equation (3). The remainder of the discussion will focus on the results for $\Delta > 1/2$. The lower broken curve in figure 1 represents, for $\Delta > 1/2$, the boundary

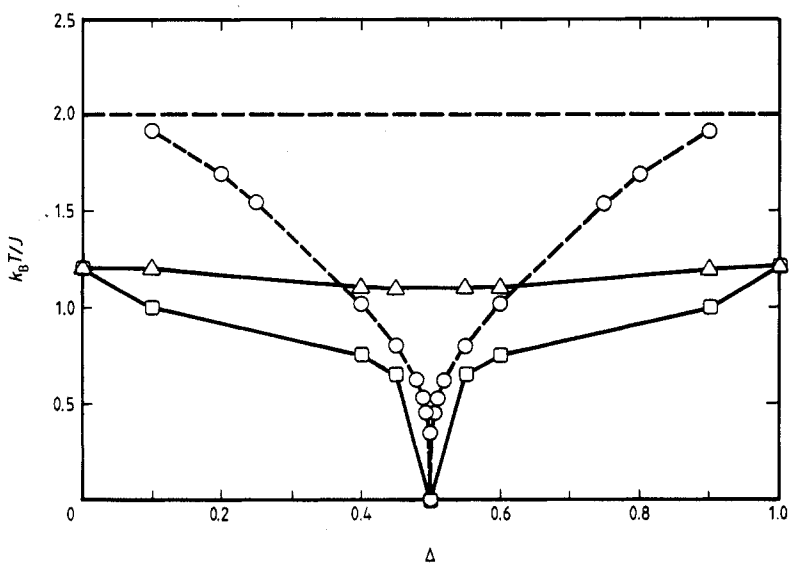

Figure 1. Large-scale features of the phase diagram of the CC_4 model from the systematic finite-lattice mean-field theory (broken curves) and Monte Carlo simulations (full curves). The upper curves in each case represent the order–disorder line T_c while the lower curves represent the boundary of the $\langle 1 \rangle$ phase. The lines connecting the points for the Monte Carlo simulations are intended as guide to the eye.

below which the $\langle 1 \rangle$ phase is the stable phase in the mean-field approximation. Along this curve, phases of the form $\langle 1^j 2 \rangle$ coexist with the $\langle 1 \rangle$ phase. This lower curve—and the value j for the coexistent phase—was determined by computing, for successive values of j, the temperature $T_{1,j}$ at which the mean-field free energies of the $\langle 1^j 2 \rangle$ phase and the $\langle 1 \rangle$ phase are identical. The phase $\langle 1^j 2 \rangle$ coexistent with $\langle 1 \rangle$ is that for which $T_{1,j}$ is a minimum.

Carrying out this procedure for various choices of Δ we find that the value of j for the phase $\langle 1^j 2 \rangle$ which is coexistent with the $\langle 1 \rangle$ phase changes at various 'branching points' as Δ increases. Thus, for example, at $\Delta = 0.505$ the phase $\langle 1^3 2 \rangle$ is coexistent with the $\langle 1 \rangle$ phase at a temperature of $T \doteq 0.459\ 062\ 856\ 452\ 62\, J/k_B$, but the phase $\langle 1^4 2 \rangle$ is not stable for this choice of Δ. However at $\Delta = 0.510$ the phase $\langle 1^4 2 \rangle$ is stable and coexists with the $\langle 1 \rangle$ phase at a temperature of $T \doteq 0.529\ 107\ 826\ 965\ 32\, J/k_B$. For a value $\Delta = \Delta_{34}$ then there is a temperature at which the three phases $\langle 1 \rangle$, $\langle 1^3 2 \rangle$ and $\langle 1^4 2 \rangle$ coexist, and this point is the 'branching point' for the $\langle 1^4 2 \rangle$ phase. For $\Delta < \Delta_{34}$ the $\langle 1 \rangle$ phase gives way, with increasing temperature, to the $\langle 1^3 2 \rangle$ phase, but for $\Delta > \Delta_{34}$ the $\langle 1 \rangle$ phase yields to the $\langle 1^4 2 \rangle$ phase. Many more branching points of this nature occur for higher values Δ, and the value of j for the phase $\langle 1^j 2 \rangle$ coexistent with the $\langle 1 \rangle$ phase can become quite large. For example, for $\Delta = 0.75$ the $\langle 1^8 2 \rangle$ phase coexists with the $\langle 1 \rangle$ phase, for $\Delta = 0.8$ the $\langle 1^{10} 2 \rangle$ phase coexists with the $\langle 1 \rangle$ phase, and for $\Delta = 0.9$ an undetermined phase $\langle 1^j 2 \rangle$ with $j > 19$ coexists with the $\langle 1 \rangle$ phase! This trend suggests the possibility that $j \to \infty$ as $\Delta \to 1$. If this is so, then the point on the $\langle 1 \rangle$ phase boundary with $\Delta = 1$ is an accumulation point [14] of the branchings of the $\langle 1^j 2 \rangle$ phases along the $\langle 1 \rangle$ phase. Note also that this proposed accumulation point coincides with the intersection of the disorder line and the $\langle 1 \rangle$ phase boundary at $\Delta = 1$.

As a first step to exploring the complex and interesting intermediate region between the mean-field $\langle 1 \rangle$ phase boundary and the mean-field order–disorder temperature $T_c = 2J/k_B$ we also determined the boundary of the $\langle 2 \rangle$ phase in the CC_4 model by a process similar to that carried out to determine the boundary of the $\langle 1 \rangle$ phase. Figure 2 shows this boundary for $\Delta > 1/2$ in relation to the $\langle 1 \rangle$ phase boundary and T_c. The boundary of the $\langle 2 \rangle$ phase was obtained by finding for successive values of j the temperature $T_{j,2}$ at which the mean-field free energies of the $\langle 12^j \rangle$ phase and the $\langle 2 \rangle$ phase are equal. The phase $\langle 12^j \rangle$ that is coexistent with the $\langle 2 \rangle$ phase is given by the value of j for which $T_{j,2}$ is a maximum. The curvature of this boundary is consistent with previous mean-field results [4, 5] for the three-dimensional CC_3 model.

The remainder of the phase diagram is filled with sequences of commensurate phases which increase in complexity as Δ increases. The temperature range over which a given phase in this region is stable is quite small and prohibits making a meaningful quantitative graph. Rather than simply making schematic plots of the phase diagram in this region, we present some typical results of the systematic finite-lattice mean-field approach in table 2, which has the further virtue of demonstrating the steps involved in the systematic mean-field approach. Each entry in table 2 represents the temperature at which G_{mf} for two phases is equal for either $\Delta = 0.505$ or $\Delta = 0.510$. From the entries in table 2 we see that for $\Delta = 0.505$ the temperature at which G_{mf} for $\langle 1 \rangle$ and $\langle 1^4 2 \rangle$ is equal is higher than the temperature at which G_{mf} for $\langle 1 \rangle$ and $\langle 1^3 2 \rangle$ are equal, signifying that $\langle 1^4 2 \rangle$ is not stable for this value of Δ. However, we see from the entries in the second column of table 2 that $\langle 1^4 2 \rangle$ is stable and coexists with the $\langle 1 \rangle$ phase at $\Delta = 0.51$.

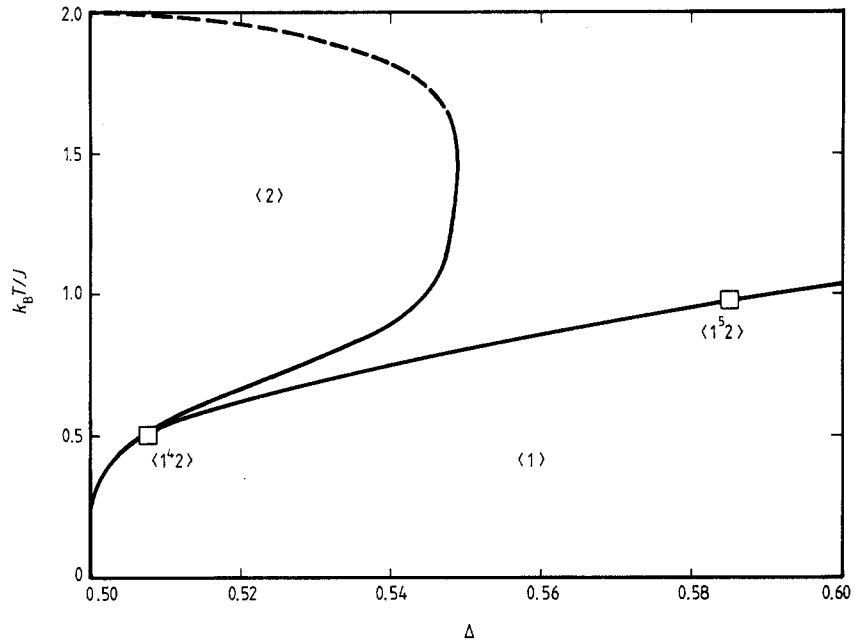

Figure 2. Phase diagram of the CC_4 model near $\Delta = 1/2$ from the systematic finite-lattice mean-field theory. The curve falling between the $\langle 1 \rangle$ boundary and T_c is the boundary of the $\langle 2 \rangle$ phase. The broken part of this boundary is an extrapolation based on the analogous part of the mean-field phase diagram of the three-dimensional CC_3 model [5]. Also shown are the approximate locations of the branching points for the $\langle 1^4 2 \rangle$ and $\langle 1^5 2 \rangle$ phases.

Table 2. Pseudo phase boundary temperatures for the CC_4 model with $\Delta = 0.505$ and $\Delta = 0.51$. The table demonstrates the way in which true phase boundaries are determined in the systematic finite-lattice mean-field approach. All temperatures are given in units of J/k_B.

	$\Delta = 0.505$	$\Delta = 0.51$
$\langle 1 \rangle : \langle 12 \rangle$	0.459 069 758 081 39	0.529 142 043 491 63
$\langle 12 \rangle : \langle 2 \rangle$	0.465 675 757 348 22	0.544 416 563 062 63
$\langle 1 \rangle : \langle 1^2 2 \rangle$	0.459 062 868 580 34	0.529 107 967 930 21
$\langle 1^2 2 \rangle : \langle 12 \rangle$	0.459 090 443 669 35	0.529 244 589 159 18
$\langle 12 \rangle : \langle 12^2 \rangle$	0.465 659 086 607 57	0.544 289 667 211 44
$\langle 12^2 \rangle : \langle 2 \rangle$	0.465 686 881 143 27	0.544 501 603 280 90
$\langle 1 \rangle : \langle 1^3 2 \rangle$	0.459 062 856 452 62	0.529 107 826 978 22
$\langle 1^3 2 \rangle : \langle 1^2 2 \rangle$	0.459 062 917 091 36	0.529 108 531 751 42
$\langle 1^2 2 \rangle : \langle 1^2 212 \rangle$	0.459 090 443 448 46	0.529 244 581 609 84
$\langle 1^2 212 \rangle : \langle 12 \rangle$	0.459 090 443 835 04	0.529 244 594 821 18
$\langle 12 \rangle : \langle 1212^2 \rangle$	0.465 659 086 444 60	0.544 289 657 335 08
$\langle 1212^2 \rangle : \langle 12^2 \rangle$	0.465 659 086 879 23	0.544 289 683 672 07
$\langle 12^2 \rangle : \langle 12^3 \rangle$	0.465 686 818 342 23	0.544 500 154 494 49
$\langle 12^3 \rangle : \langle 2 \rangle$	0.465 686 906 263 80	0.544 502 182 838 75
$\langle 1 \rangle : \langle 1^4 2 \rangle$	0.459 062 856 453 09	0.529 107 826 965 32
	⋮	

The systematic finite-lattice mean-field analysis of the CC_8 model is much more difficult than that of the CC_4 model because the number of stable phases for a given Δ increases, and this in turn leads to larger and larger lattices to accommodate the hypothesised phases. We have for this reason restricted our mean-field analysis in this instance to determining the $\langle 1 \rangle$ phase boundary. This boundary is shown in figure 3. As in figure 1 for the CC_4 model, figure 3 also shows the results of Monte Carlo simulations for the CC_8 model to be described in the next section. Note that the $\langle 1 \rangle$ boundary for the CC_8 model is suppressed relative to the same boundary for the CC_4 model.

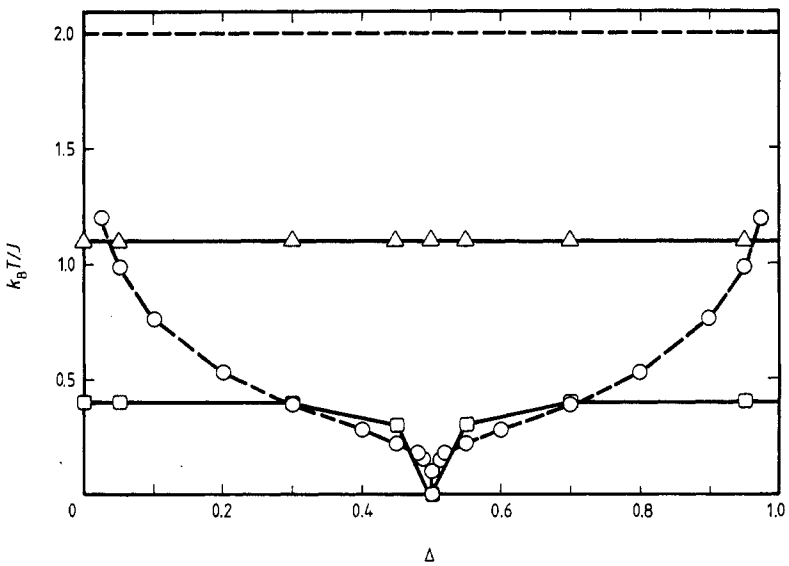

Figure 3. Large-scale features of the phase diagram of the CC_8 model from the systematic finite-lattice mean-field theory (broken curves) and Monte Carlo simulations (full curves). The upper curves in each case represent the order–disorder line T_c while the lower curves represent the boundary of the $\langle 1 \rangle$ phase. The mean-field $\langle 1 \rangle$ boundary rises to intersect the mean field T_c at $\Delta = 0$ and $\Delta = 1$. The lines connecting the points for the Monte Carlo simulations are intended as a guide to the eye.

3. Monte Carlo studies

3.1. Method

The Monte Carlo (MC) calculations were carried out in a manner very similar to the calculations of Selke and Yeomans [7] for the two-dimensional CC_3 model. In particular, the Hamiltonian of equation (1) was used to define the model on a lattice of 132 sites along the chiral (z) axis by 32 sites along the perpendicular axis. Periodic boundary conditions were imposed, and the standard Monte Carlo sampling algorithm was used [16]. Full simulations were carried out for models with $p = 4$ and $p = 8$, and for $0.5 < \Delta < 0.95$, taking advantage of the symmetry of the partition function (3). Each run was initially started from the chiral ground state or from an equilibrated configuration generated at a slightly different temperature. Generally, systems were equilibrated for (0.5–2) $\times 10^4$ MC steps per site, and averages were calculated over

$(1.5–3) \times 10^4$ per site, or until averages appeared stable. Quantities calculated included the average energy of the system, the specific heat using the energy fluctuation relation [16] and the average value of the Potts variable in each row as a function of the location z along the chiral axis. In addition, 'snapshots' of configurations were examined at intermediate points in each run.

3.2. Monte Carlo results

The usual way of locating phase boundaries, via anomalies in the specific heat, did not prove to be useful for the values of p used in the simulations. Generally plots of specific heat against T were broad with only a hint of a 'shoulder' at a temperature close to the onset of the modulated phase. We found more dramatic evidence for phase changes in plots of $\langle n_z \rangle_{\text{row}}$ as functions of z. A sequence of such plots for $p = 4$ and $\Delta = 0.55$ is shown in figure 4, which demonstrates that at $T \leq 0.4\,J/k_B$ the system remains in the ground state chiral phase. However, at $T = 0.9\,J/k_B$ the plots change to patterns indicative of modulated order. This is evidenced by the different periodicities of the plots and by the correlation between averages at some neighbouring sites (two NN sites having nearly the same $\langle n_z \rangle_{\text{row}}$). At $T = 1.1\,J/k_B$ all the averages are very close to the fully disordered value, which is 1.5 for $p = 4$. We have used these signatures in the order parameter plots to approximately locate the phase boundaries by examining averages calculated for $\Delta = 0.55$, 0.6 and 0.9. The resulting phase diagram is shown by the full curves in figure 1. The points for $\Delta < 1/2$ were obtained by reflection about the line $\Delta = 1/2$.

To further ascertain the nature of the modulated region, examination of individual configurations is helpful. Table 3 shows a series of such configurations. Evidence of overlapping regions of modulated phase sequences of the form $\langle 1^j 2^k \rangle$ is seen in table 3(*b*). These sequences do not appear above $T \simeq 1.1\,J/k_B$ (table 3(*c*)) or at low temperatures (table 3(*a*)).

The calculations for the $p = 8$ model were carried out in the same fashion as the $p = 4$ model above. Again, the phase boundaries were best determined by examining the plots of $\langle n_z \rangle_{\text{row}}$ against z. Figure 5 shows a sequence of these plots for $\Delta = 0.55$. Note that the modulated phase sets in at a lower temperature than in the four-state model. Figure 3 shows, together with the mean-field results described earlier, the phase diagram obtained from order parameter plots. For large p the modulated phase persists down to $\Delta = 0$. Direct MC simulations at $\Delta = 0$ confirm that a change occurs in the order parameter plots at $T = 0.4\,J/k_B$ as figure 5 indicates, but examination of the configurations shows no easily discernible modulation patterns. The nature of the intermediate phase at $\Delta = 0$ or $\Delta = 1$ is not known. Table 4 shows snapshots of configurations found in the modulated region for $\Delta = 0.95$, revealing an example of the nature of the phases in this region. Configurations in the modulated phase region (table 4(*b*)) show regions of $\langle 1^j 2 \rangle$ phases for various values of j.

4. Comparison of the two methods and conclusions

To compare the results of the mean-field and Monte Carlo methods for the two-dimensional CC_p model, consider once again figure 1 which shows the phase diagrams for the CC_4 model obtained by the two methods. Near the multiphase point the Monte Carlo calculations are not sufficiently accurate to pin down the width of the modulated region (the lines connecting the calculated phase-change points in the Monte Carlo

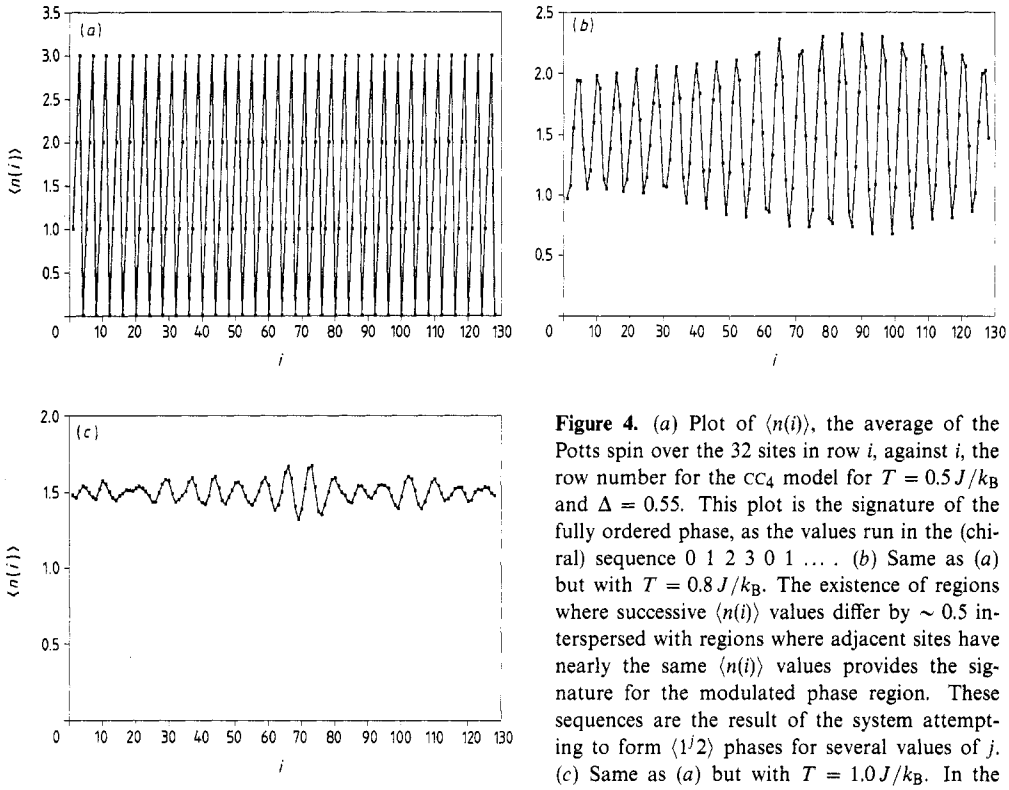

Figure 4. (*a*) Plot of $\langle n(i)\rangle$, the average of the Potts spin over the 32 sites in row i, against i, the row number for the CC_4 model for $T = 0.5J/k_B$ and $\Delta = 0.55$. This plot is the signature of the fully ordered phase, as the values run in the (chiral) sequence 0 1 2 3 0 1 ... . (*b*) Same as (*a*) but with $T = 0.8J/k_B$. The existence of regions where successive $\langle n(i)\rangle$ values differ by ~ 0.5 interspersed with regions where adjacent sites have nearly the same $\langle n(i)\rangle$ values provides the signature for the modulated phase region. These sequences are the result of the system attempting to form $\langle 1^j 2\rangle$ phases for several values of j. (*c*) Same as (*a*) but with $T = 1.0J/k_B$. In the fully disordered phase all values of n are equally likely at any site, so all averages should converge to 1.5, the arithmetic average of 0 1 2 3. This is very nearly the case for the model at this temperature.

portion of the diagram are intended as guides to the eye) but the two diagrams agree fairly well in this area. The location of the line separating the disordered phase from the modulated phases is higher in the mean-field approximation than in the computer simulations, and this overestimate is typical of the mean-field approximation. The comparison of the phase diagrams that result from the two methods for the CC_8 model is shown in figure 3. As was the case for the CC_4 model calculations, the methods are in reasonable agreement for the location of the modulated phase line in the region of the multiphase point, with the mean-field method predicting a substantially higher modulated–disordered phase transition line than the Monte Carlo method. When comparing the mean-field and Monte Carlo methods it is important to remember the role of dimensionality in the two methods. In the mean-field approximation, the dimensionality enters in only through the coordination number. For the CC_p model this means that commensurate phases are found in mean-field theory even for $d = 2$. In the Monte Carlo simulations the algebraic decay of correlations [1] in the two-dimensional CC_p model inhibits the appearance of such phases. Thus the two methods differ in the precise nature of the modulated region of the phase diagram.

A qualitative difference between the CC_4 and CC_8 models is seen by comparing figures 1 and 3. In figure 1 for the CC_4 model, the boundary of the $\langle 1\rangle$ phase in both the mean-field and Monte Carlo methods rises to approach the order–disorder line and

Table 3. Typical configurations generated in the Monte Carlo simulations of the CC_4 model. In all configurations, $\Delta = 0.6$. (*a*) Configuration for $T = 0.4\,J/k_B$ showing chiral order. (*b*) Configuration for $T = 0.9\,J/k_B$ showing the modulated region. Simple structures do not appear because of the very small free-energy differences between modulated phases. Rather, one sees small regions where $\langle 1^J 2 \rangle$ phases begin to form, along with more complicated phases. (*c*) Configuration for $T = 1.1\,J/k_B$ showing a more or less random distribution of Potts spin values throughout the lattice.

(*a*) $T = 0.5\,J/k_B$

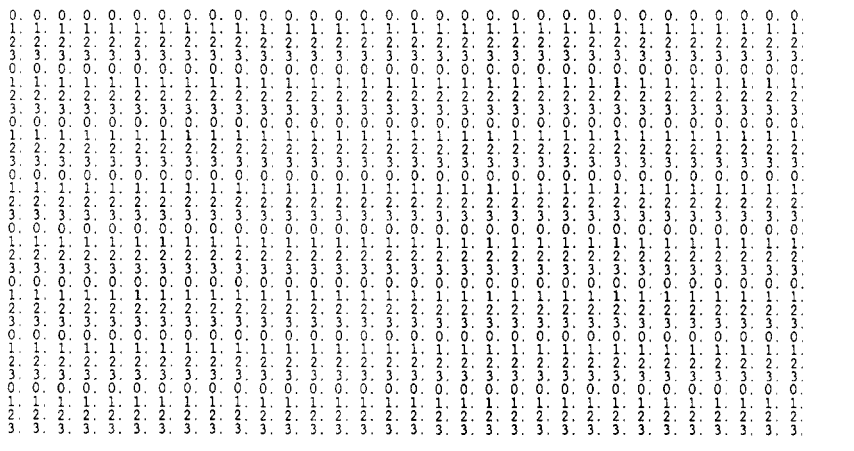

(*b*) $T = 0.8\,J/k_B$

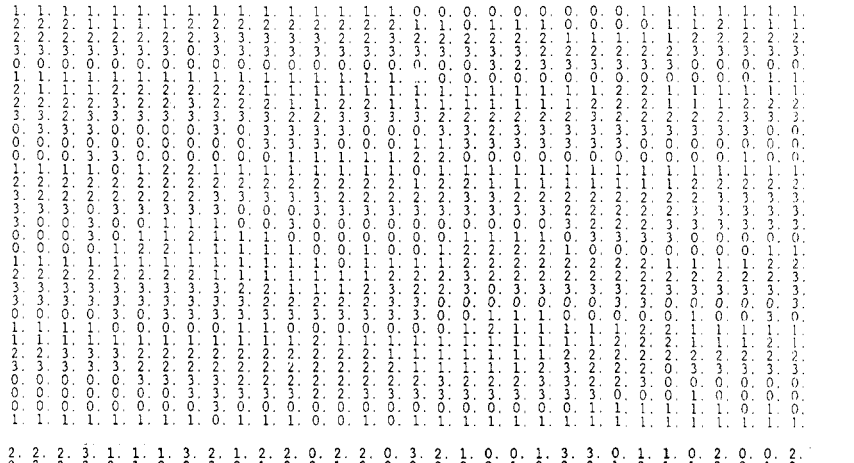

(*c*) $T = 1.0\,J/k_B$

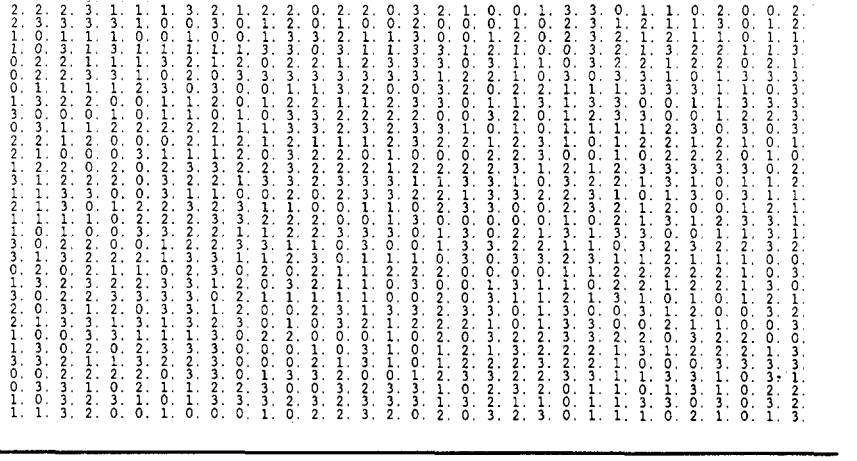

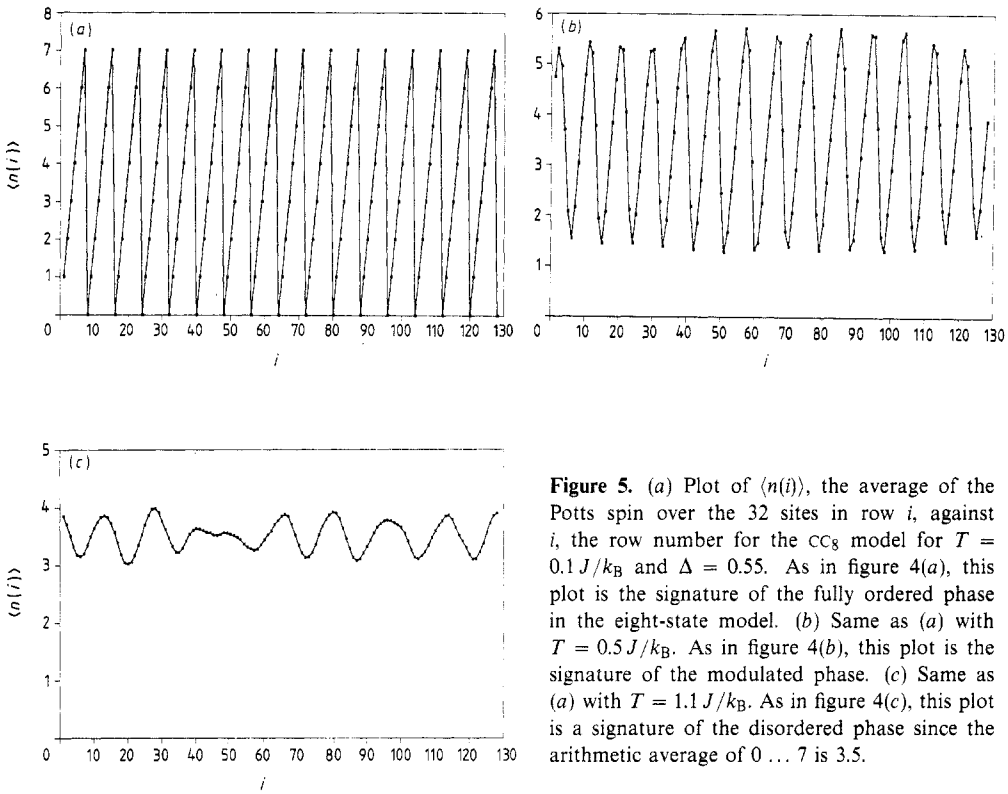

Figure 5. (*a*) Plot of $\langle n(i) \rangle$, the average of the Potts spin over the 32 sites in row i, against i, the row number for the CC_8 model for $T = 0.1\,J/k_B$ and $\Delta = 0.55$. As in figure 4(*a*), this plot is the signature of the fully ordered phase in the eight-state model. (*b*) Same as (*a*) with $T = 0.5\,J/k_B$. As in figure 4(*b*), this plot is the signature of the modulated phase. (*c*) Same as (*a*) with $T = 1.1\,J/k_B$. As in figure 4(*c*), this plot is a signature of the disordered phase since the arithmetic average of 0 ... 7 is 3.5.

apparently intersects T_c at $\Delta = 1.0$ and $\Delta = 0.0$. In figure 3 for the CC_8 model, however, MC simulations carried out at $\Delta = 0$ show that the ordered low-temperature phase undergoes fluctuations over the size of the simulation cell when T is increased above about 0.35, and below this temperature the system remains locked in the fully ordered phase. The system does not become fully disordered, however, until $T \simeq 1.1\,J/k_B$, even when $\Delta = 0$. Thus it would appear from the simulations that for the two-dimensional CC_8 model an intermediate phase persists even at $\Delta = 0$. This is in basic agreement with the results of the free-fermion approximation for the two-dimensional CC_p model as found earlier by Ostlund [1]. In the free-fermion approximation an intermediate phase persists down to $\Delta = 0$ only for $p \geq 5$. The Monte Carlo simulations are then in qualitative agreement with the results of the free-fermion approximation. The fact that the modulated phases do not persist at $\Delta = 1$ (or equivalently at $\Delta = 0$ by equation (3)) in the mean-field theory of the two-dimensional CC_8 model suggests that the free-fermion approximation is a better approximation in this region than is the mean-field approximation. We note also that the prediction of an intermediate phase at $\Delta = 0$ in the free-fermion approximation of the chiral clock model for $p \geq 5$ is in agreement with recent general results for models with $Z(p)$ symmetry [17], which include the chiral clock model at $\Delta = 0$. Bonnier *et al* [17] found that the $Z(p)$-symmetric transition is of the Kosterlitz–Thouless type [18] for $p \geq 5$ and of the Ising type for $p < 5$.

Although the Monte Carlo simulations confirm the results of the free fermion approximation, no *simple* phase structure emerges from the calculations in the modulated regions. This is perhaps due in part to the finite lattice size chosen for the Monte Carlo simulations, but this of course is a potential problem in any Monte Carlo sim-

Table 4. Typical configurations generated in the Monte Carlo simulations of the CC_8 model. In these configurations, $\Delta = 0.95$. As in table 3, a configuration typical of each phase region is shown. (*a*) Configuration for $T = 0.1\,J/k_B$. (*b*) Configuration for $T = 0.4\,J/k_B$. (*c*) Configuration for $T = 1.1\,J/k_B$.

(*a*) $T = 0.1\,J/k_B$

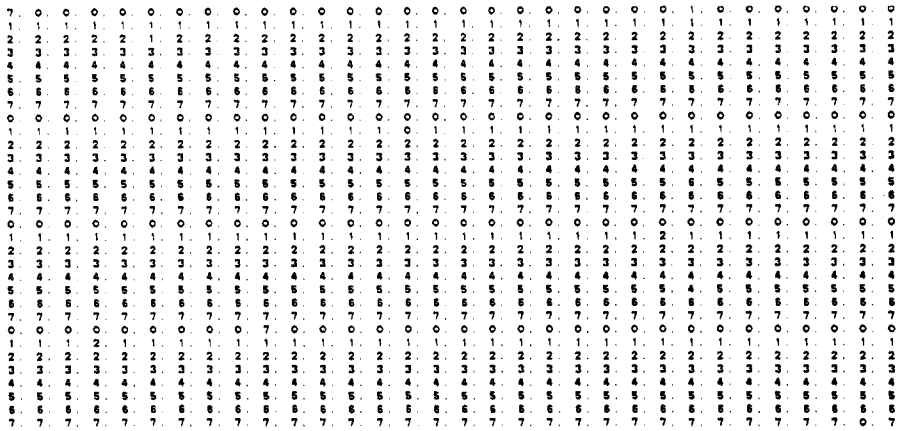

(*b*) $T = 0.4\,J/k_B$

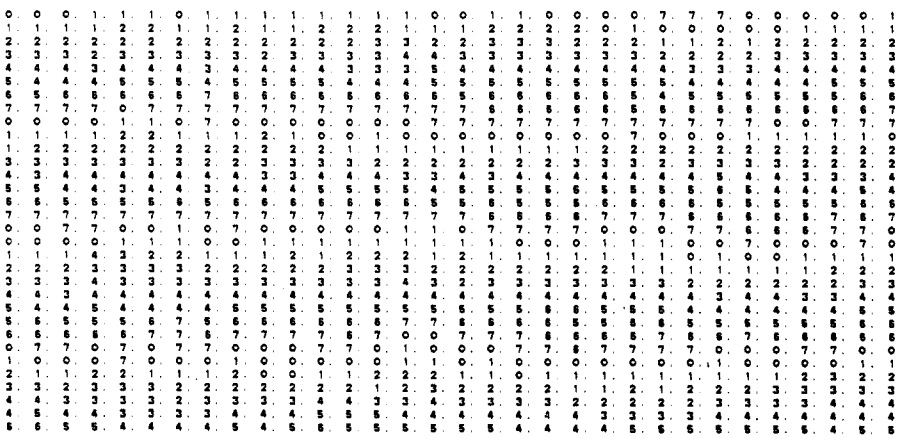

(*c*) $T = 1.1\,J/k_B$

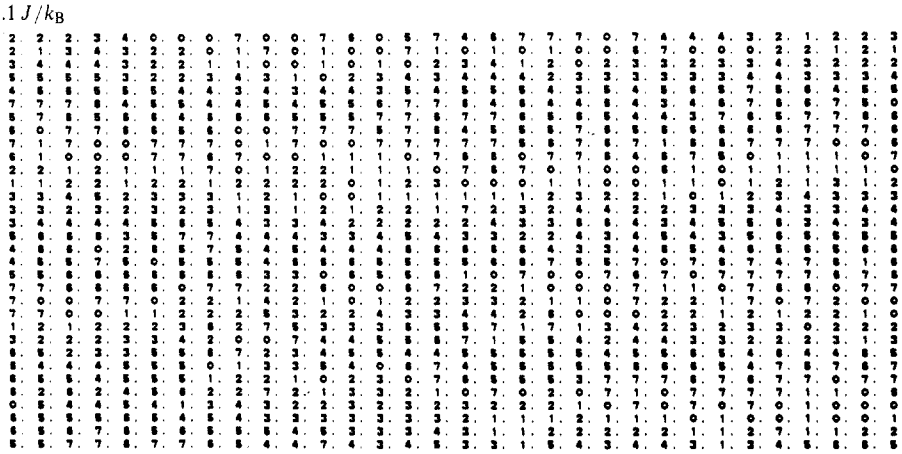

ulation. The problem of identifying specific commensurate phases from Monte Carlo simulations merits further investigation. Furthermore, the multiple-state nature of the CC_p model for $p > 5$ makes identification of statistically meaningful and physically relevant local dislocations or defects very difficult. Such an identification is needed to determine whether the models fit the Kosterlitz–Thouless picture of two-dimensional disorder transitions.

Acknowledgments

The authors wish to thank Professor John Chandler for helpful discussions regarding the numerical analysis of the mean-field equations, and Professor Jacques Perk for his comments on the contents of this manuscript. HLS was supported by NSF grant DMB 8703644. The authors gratefully acknowledge the support of the National Science Foundation through grant DMB 8703644.

References

[1] Ostlund S 1981 *Phys. Rev.* B **24** 398
[2] Huse D 1981 *Phys. Rev.* B **24** 5180
[3] Yeomans J and Fisher M E 1984 *Physica* **127A** 1
[4] Öttinger H C 1982 *J. Phys. C: Solid State Phys.* **15** L1257; 1983 *J. Phys. C: Solid State Phys.* **16** L257, L597
[5] Siegert M and Everts H 1985 *Z. Phys.* B **60** 265
[6] Siegert M and Everts H 1987 *Z. Phys.* B **66** 227
[7] Selke W and Yeomans J 1982 *Z. Phys.* B **46** 311
[8] Selke W 1988 *Phys. Rep.* **170** 213
[9] Yeomans J 1982 *J. Phys. C: Solid State Phys.* **15** 7305
[10] Scott H L Jr and Pearce P A 1989 *Biophys. J.* **55** 339
[11] Zasadzinski J A N, Schneir J, Gurley J, Elings V and Hansma P K 1988 *Science* **239** 1013
[12] Falk H 1970 *Am. J. Phys.* **38** 858
[13] Yokoi C, Coutinho-Filho M and Salinas S 1981 *Phys. Rev.* B **24** 4047
[14] Selke W and Duxbury P 1984 *Z. Phys.* B **57** 49
[15] Press W, Flannery B, Teukolsky S and Vetterling W 1986 *Numerical Recipes* (Cambridge: Cambridge University Press)
[16] Binder K (ed) 1986 *Monte Carlo Methods in Statistical Physics* 2nd edn (Berlin: Springer); 1987 *Applications of the Monte Carlo Method in Statistical Physics* 2nd edn (Berlin: Springer)
[17] Bonnier B, Hontebeyrie M and Meyers C 1989 *Phys. Rev.* B **39** 4079
[18] Kosterlitz J M and Thouless D J 1973 *J. Phys. C: Solid State Phys.* **6** 1181